Missouri University of Science and Technology
Scholars' Mine

NASA-Missouri Space Grant Consortium

Apr 22nd, 8:30 AM - 10:00 AM

# Computations of Flow past a Three-Element 30P30N Airfoil Using Wray-Agarwal One Equation Turbulence Model

Karsten Hendrickson
*Washington University in St. Louis*

Follow this and additional works at: https://scholarsmine.mst.edu/nmsgc

Hendrickson, Karsten, "Computations of Flow past a Three-Element 30P30N Airfoil Using Wray-Agarwal One Equation Turbulence Model" (2023). *NASA-Missouri Space Grant Consortium*. 25.
https://scholarsmine.mst.edu/nmsgc/2023/full-schedule/25

This Presentation is brought to you for free and open access by Scholars' Mine. It has been accepted for inclusion in NASA-Missouri Space Grant Consortium by an authorized administrator of Scholars' Mine. This work is protected by U. S. Copyright Law. Unauthorized use including reproduction for redistribution requires the permission of the copyright holder. For more information, please contact scholarsmine@mst.edu.

# Computations of Flow past a Three-Element 30P30N Airfoil Using Wray-Agarwal One Equation Turbulence Model

**Karsten Hendrickson**
**Washington University in St. Louis**
**Dr. Ramesh Agarwal**

## Abstract

The predictions of flow phenomenon that occur in high lift systems have proven to be challenging using the Reynolds-Averaged Navier-Stokes (RANS) equations with turbulence models. The complex interactions that occur among different elements of the wing can be difficult for turbulence models to accurately predict. Results from the recently developed Wray-Agarwal (WA) one-equation turbulence model, the frequently used Spalart-Allmaras (SA) and shear stress transport (SST) k-ω turbulence models are compared to experimental results to evaluate each model's relative accuracy. The quadratic constitutive relation (QCR) is also used to produce results with the SA and WA models. It is shown that at lower angles of attack the computed lift from each turbulence model has similar accuracy as in the experimentally determined lift. At higher angles of attack, the WA model shows decreased accuracy while the SA and SST k-ω have similar accuracy. For other computed flow field quantities, the experimental data generally matches closest to the results from the SA model on a fine grid. In some cases, the WA and SST k-ω model have improved accuracy over the SA model on the same grid.

## Introduction

The accurate prediction of high lift flows presents a significant challenge for computational fluid dynamics (CFD) codes. There can be many complex physical effects that need to be correctly modeled including flow in regions of large pressure gradients, the wake and merging of wake and boundary layers, unsteady flow, separated flow and laminar/turbulent transition on different wing elements [1,2]. This problem is further amplified at higher angles of attack where the difficulty is compounded in accurately predicting the flow field due to separation and possible stall.

In the literature, many investigations have been reported on evaluating the ability of different turbulence models in accurately predicting the high lift flows. A survey by Rumsey and Ying in 2002 [1] summarizes the CFD analysis of high lift systems over a period of 10-15 years before 2000; they proposed three possible reasons for inaccurate CFD predictions of high lift flows: "(1) unsteady effects, (2) inadequacy of turbulence models, and (3) numerical errors and lack of geometric or modeling fidelity" [1]. The advances in computing power in last 20-30 years have allowed for larger meshes and improved geometric fidelity. As a result, the understanding of relative contribution of unsteady effects and inadequate turbulence modeling to the total error in CFD prediction of high lift flows has become more significant.

Previous research has shown that Reynolds-Averaged Navier-Stokes (RANS) equations with several turbulence models are capable of predicting lift, drag, surface pressures, and skin friction over multi-element airfoils with good accuracy for angles of attack below stall; however at angles of attack above stall, RANS simulations are unable to predict these quantities accurately [1,2] because of unsteady nature of the flow at stall and the experiments also cannot be considered as nearly two dimensional. Rumsey and Ying [1] found that, with some exceptions,

most RANS models can successfully predict the surface pressures and general flow field quantities such as velocity profiles in 2D high lift flows with sufficient accuracy at relatively modest mesh densities of 100,000-200,000 points [1]. An exception to this is the k-ε turbulence model which was shown to have difficulty in accurately predicting the wall bounded flows in adverse pressure gradient [1]. Different turbulence models can also have inconsistent levels of accuracy in predicting different flow phenomenon. Ashton et al. [3] observed in their analysis of 30P30N high lift three element airfoil that despite each turbulence model predicting similar levels of lift, the lift contribution by each element was different for each turbulence model. Takeda et al. [4] found that the SA turbulence model showed better agreement with experimental results on the upper side of the 30P30N airfoil while the SST k-ω turbulence model showed better agreement in the slat cove. Additionally, while the velocity profiles in the flow are accurately predicted in most of the domain, the prediction of complex flow field in slat region and flap region can suffer from inaccuracies compared to experimental data. This is most noticeable in prediction of wakes from upstream elements.

The accurate prediction of the interaction between the wake of an upstream element and the boundary layer of a downstream element has proven very difficult for RANS models. This is most significant with the slat wake and can lead to additional errors downstream. This complex merging can extend well beyond the airfoil surface, reaching as far as 20% of the chord length above the flap [5]. In a summary of past CFD analysis of 2D high lift flows, Rumsey and Ying [1] noted that the slat wake was consistently predicted too be larger and wider than in experimental results. The merging of the multiple viscous layers is a complex phenomenon and has been a topic of considerable research. At low angles of incidence this merging can be very quick with flow being fully merged at the main element mid-chord [6], while at high angles of incidence the layers can remain unmerged past the trailing edge of the flap [5].

The comparison between experimental and computation analysis of 2D geometries remains challenging as 3D effects often arise in experimental testing, especially with high lift multi-element geometries. Boundary layers on the walls of the wind tunnel can cause span-wise variations along the wing [7]. While this is generally not an issue at low angles of incidence, at higher angles of incidence the boundary layers can induce separation earlier than would be seen in a truly 2D flow. This separation can cause massive span-wise variation in the flow field making it difficult to determine an accurate level of lift for the wing. In order to counter these effects Rumsey et al. [7] introduced wall venting with the goal of limiting the boundary layer growth along the wind tunnel walls. They found that venting increased the coefficient of lift by 0.1-0.2 at all angles of attack. However, they were still not able to achieve uniform span-wise flow at high angles of attack and the stall angle did not change between vented and non-vented flow. Perhaps, it can be concluded that differences between CFD and experimental data at high angles of incidence can be the result of errors both in numerical modeling and experimental measurement.

The goal of this paper is to perform numerical simulations on the MD 30P30N three element airfoil and compare the results to available experimental data. The recently developed Wray-Agarwal (WA2017) turbulence model [8], Spalart-Allmaras (SA) and Shear-Stress-Transport (SST) k-ω turbulence models are used to evaluate their relative accuracy for predicting 2D high lift flows. In addition to the linear versions of the turbulence models, the quadratic constitutive

relation (QCR) [9] is used with the SA and WA turbulence models to evaluate the efficacy of a higher order eddy viscosity relation for these models.

**Wray-Agarwal Turbulence Model**

The Wray-Agarwal (WA) model is a newly developed one-equation eddy-viscosity turbulence model derived from k-ω closure. In this model, a new variable $R$ is introduced which is defined as $k/\omega$. It has been applied to several canonical flows [10] and has shown improved accuracy over the SA model and competitiveness with the SST $k$-$\omega$ model. An important distinction between the WA model and previous one-equation models based on two equation $k$-$\omega$ models is the inclusion of the cross-diffusion term in the $\omega$-equation and a blending function which allows smooth switching between two destruction terms. The equations of the WA turbulence model are given below.

$$\frac{\partial R}{\partial t} + u_j \frac{\partial R}{\partial x_j} = \frac{\partial}{\partial x_j}\left[(\sigma_R R + \nu)\frac{\partial R}{\partial x_j}\right] + C_1 RS + f_1 C_{2k\omega}\frac{R}{S}\frac{\partial R}{\partial x_j}\frac{\partial S}{\partial x_j} - (1-f_1)C_{2k\varepsilon}R^2\left(\frac{\frac{\partial S}{\partial x_j}\frac{\partial S}{\partial x_j}}{S^2}\right) \quad (1)$$

$$f_1 = tanh(arg_1^4) \quad (2)$$

$$arg_1 = \frac{1+20\eta}{1+\left(\frac{d\max\left(\sqrt{RS},1.5\right)}{20\nu}\right)^2} \quad (3)$$

$$\eta = \frac{d\sqrt{RS}}{20\nu} \quad (4)$$

The eddy viscosity is calculated through the new variable $R$

$$\nu_t = f_\mu R \quad (5)$$

Again, to account for the wall blocking effect, the damping function $f_\mu$ is defined in the same form of SA model.

$$f_\mu = \frac{\chi^3}{\chi^3 + C_w^3}, \qquad \chi = \frac{R}{\nu} \quad (6)$$

While the $C_{2k\omega}$ term is active, Eq. (2.3.1) behaves as a one equation model based on the standard $k$-$\omega$ equations. The inclusion of the cross-diffusion term in the derivation causes the additional $C_{2k\varepsilon}$ term to appear. This term corresponds to the destruction term of one equation models derived from standard $k$-$\varepsilon$ closure. The presence of both terms allows the new model to behave either as a one equation $k$-$\omega$ or one equation $k$-$\varepsilon$ model based on the switching function $f_1$. Being a one equation model, it is more computationally efficient than the multi-equation models. Even though the WA model appears promising, it also has limitations in accuracy for computing wall bounded separated flows.

**Quadratic Constitutive Relation (QCR)**

Quadratic Constitutive Relation (QCR) is utilized to have a non-linear relationship between stress and strain tensor for turbulent eddy viscosity with the goal of achieving better prediction of the highly separated flow at high angles of incidence. This method is described by Spalart [9] and is commonly referred to as QCR2000. The eddy viscosity is computed as normal but instead of the traditional linear Boussinesq relation, the turbulent stress is computed using the following relation:

$$\tau_{ij,QCR} = \tau_{ij} - C_{cr1}\left[O_{ik}\tau_{jk} + O_{jk}\tau_{ik}\right] \quad (7)$$

where $\tau_{ij}$ denotes the turbulent stresses computed using the linear Boussinesq relation, and $O_{ik}$ is an antisymmetric normalized rotation tensor defined as:

$$O_{jk} = 2W_{ik} / \sqrt{\frac{\partial u_m}{\partial x_n}\frac{\partial u_m}{\partial x_n}} \quad (8)$$

$$W_{ik} = \frac{1}{2}\left(\frac{\partial u_i}{\partial x_k} - \frac{\partial u_k}{\partial x_i}\right) \quad (9)$$

In Eq. (9), the constant $C_{cr1} = 0.3$. The model is implemented in ANSYS Fluent using a User-Defined Function (UDF). In order to improve the stability of flows computed using the QCR model, the limited velocity gradients are used. Analysis on a 2D flat plate and 2D bump geometries found the effects of the gradient limiters to be negligible.

**Physical Model**

The MDA 30P30N is a three-element airfoil developed by McDonnell Douglas for which a considerable amount of experimental and numerical analysis has been performed. The geometry and parameters of the 30P30N are presented in **Error! Reference source not found.** and Table 1.

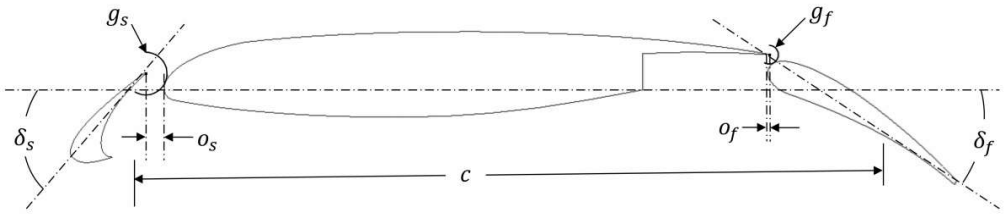


**Figure 1 Definition of parameters of the 30P30N geometry**

**Table 1 Parameters of the 30P30N geometry**

| Geometric Parameter | Value |
|---|---|
| Stowed Chord (c) | 1 m |
| Slat Deflection (δs) | 30 deg |
| Slat Gap (GS) | 2.95% |
| Slat Overhang (os) | -2.50% |
| Flap Deflection (δf) | 30 deg |
| Flap Gap (gf) | 1.27% |
| Flap Overhang (of) | 0.25% |

A square 2D domain was generated with a far field extending to 100 chord lengths in each direction and is shown in Figure 2. This domain was extruded one cell's width in the Z direction resulting in a quasi-2D analysis. A freestream Mach number of 0.2 was selected resulting in a Reynolds number of approximately $9 \times 10^6$.

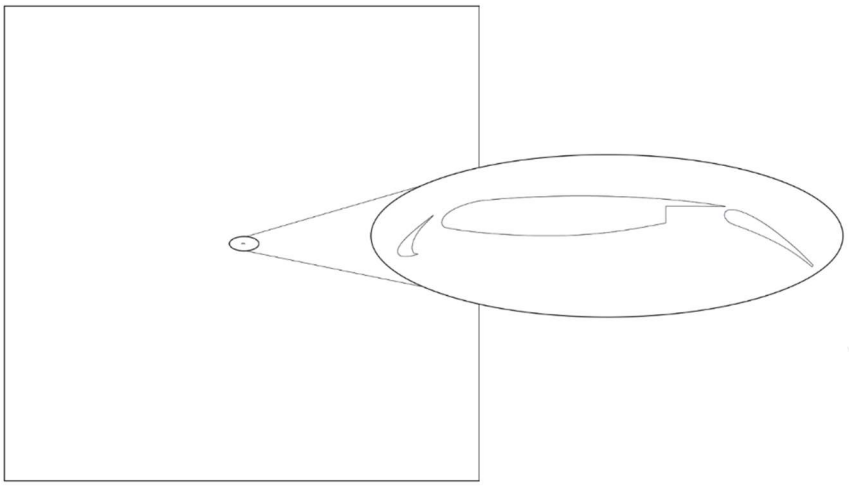

**Figure 2 Computational Domain**

## Numerical Methods

The compressible RANS equations are solved using a pressure-based solver with the SA, SST k-ω, and WA turbulence models. In addition to the conventional models, the Quadratic Constitutive Relation is used for the SA and WA turbulence models. Sutherland's law is used to calculate viscosity and density is calculated using the ideal gas law. The coupled scheme is used for the pressure-velocity coupling. Second order upwind schemes are used for the convection terms in fluid conservation equations and turbulence model equations. The least squares cell based gradient discretization is used for the SA and SST k-ω models while the Green-Gauss node based scheme is used for the WA model as it resulted in better accuracy for the WA model and was found to be more stable by Drikakis et al. [11] for high aspect ratio elements such as the ones seen in the boundary layers. A freestream value of $R=4\nu_\infty$ is used at the farfield boundary conditions while $R=0$ is enforced at the walls.

A mesh independence study was performed at 8 degrees angle of attack to evaluate the effects of mesh density on each turbulence model. Five meshes, ranging from extra coarse to very fine, were generated using the gridding guidelines published for the 3rd AIAA High lift Prediction Workshop [12]. Details for each grid are given in Table 2. Figure 3 shows the structured grid around the 30P30N airfoil and zoomed-in-view of the mesh in the gaps between the elements.

**Table 2 Details of each mesh level**

| Mesh Level | Cells | Y+ | Initial Wall Spacing ΔY |
|---|---|---|---|
| Extra Coarse | 244476 | 1.5 | 0.06223 mm |
| Coarse | 435118 | 1.0 | 0.03793 mm |
| Medium | 1071608 | 2/3 | 0.02599 mm |
| Fine | 2411496 | 4/9 | 0.01447 mm |
| Very Fine | 5424792 | 8/27 | 0.01321 mm |

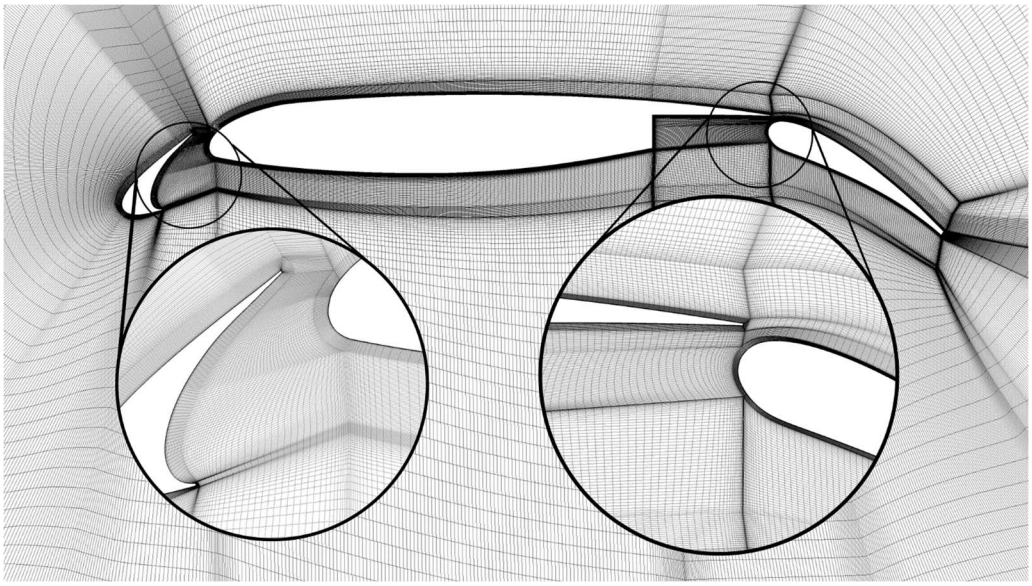

**Figure 3 Computational grid around 30P30N and close-up of element interfaces**

## Results

The coefficients of total lift, lift for each element, total drag, and skin friction at two test points are computed on a series of increasing grid densities using each turbulence model. The results are shown in Figure 4 and Figure 5 and are compared to the experimental results provided by Chin et al. [13]. The SA model slightly over-predicts both the total lift and the lift generated by each element. The total lift and main-element lift predicted by the SST $k$-$\omega$ model is slightly under-predicted while the lift predicted for the two other elements is slightly over-predicted. Results using the SST $k$-$\omega$ model also show the best agreement with experimental results. The total lift and lift produced by the flap and main elements are all under-predicted by the WA model. On coarser meshes the value of lift is in significant disagreement with experimental results, however on the finest mesh, results are better than those predicted by the SA model and nearly in as good of agreement as those predicted by the SST $k$-$\omega$ model. The lift generated by the slat is under-predicted by the WA model on the coarsest mesh but follows a similar trend to the other lift values and ultimately over-predicts the lift by slightly less than the SA and SST $k$-$\omega$ models. As the grid is refined, the SST $k$-$\omega$ model demonstrates a slight increase in the measured lift values while the SA model results remain steady. The lift results for the SA-QCR and WA-QCR models are also plotted. The general trends for each model match that of their linear base models. In both cases the use of QCR results in a slight decrease in the measured lift values. For the SA model this results in improved agreement as the lift values are initially over-predicted. For the WA model this results in a decrease in agreement with the experimental results as the base model under-predicts lift values. The WA-QCR model sees a greater change in the measured lift as the grid density is increased when compared to all other turbulence models. This may be a result of using a limited gradient when computing the non-linear Reynolds stress terms in the QCR model, as the reduced accuracy in areas with a high velocity gradient will require additional grid density for the flow to be adequately resolved. Plots of the coefficient of drag indicate significant disagreement between all three turbulence models, their corresponding QCR versions, and experimental results. It is unclear what the primary cause is for this large difference. When considering the relative accuracy of various other computed results when

compared to experimental measurements, it seems reasonable to expect that computed drag would at least show modest agreement with experimental results, especially at a low angle of attack, where the amount of separated flow is relatively low. An over prediction of drag coefficient is consistent with previous high lift flow field simulations reported in the literature [1,14,15]; however, the magnitude of over prediction in drag coefficient is relatively larger in the present simulations.

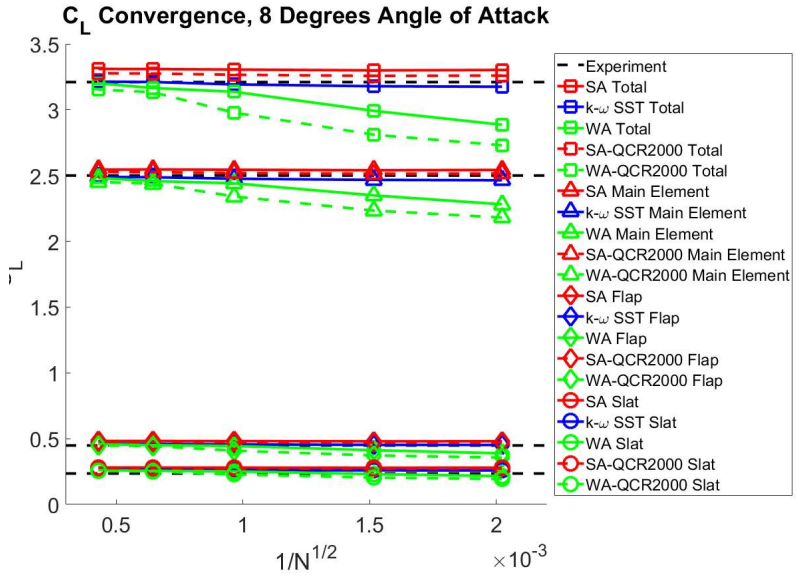


**Figure 4 Lift convergence for SA, SST k-ω, WA, SA-QCR2000, and WA-QCR2000 turbulence models, 8 degrees angle of attack**

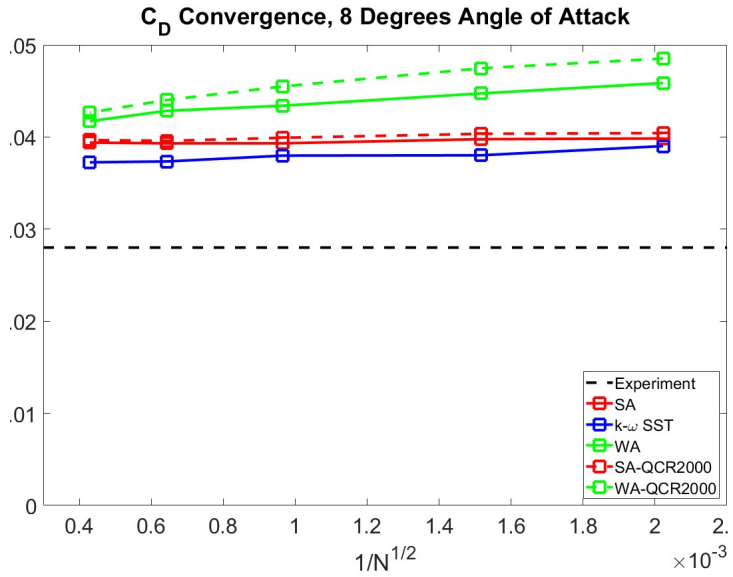


**Figure 5 Drag convergence for SA, SST k-ω, WA, SA-QCR2000, and WA-QCR2000 turbulence models, 8 degrees angle of attack**

The coefficients of skin friction at locations close to the trailing edge of the main element (x/c = 0.825) and flap (x/c = 1.094), computed for each grid density and using each turbulence model are shown in Figure 6. The computed results are compared to experimental results provided by Klausmeyer and Lin [16]. While initially the SST *k-ω* model shows good agreement with experimental results, as the grid is refined, the predicted skin friction at both the main element and slat probes decreases, and agreement with experimental results becomes poor. At the main element probe the WA model shows a similar trend of decreasing skin friction, however this is shifted above the experimental value, resulting in improved agreement as the grid is refined. At the finest two grid densities both the SA and WA models show nearly identical levels of agreement with experimental results. Skin friction predicted at the flap probe by both the WA and SA models increases as the grid is refined resulting in poor agreement with the experimental value for the finest grid, especially for the WA model. At the main element probe the use of QCR results in improved agreement between computed and experimental results for all grid levels. At the finest grid density, the SA-QCR and WA-QCR models once again predict identical levels of skin friction. Along the flap probe the SA-QCR and WA-QCR models predict identical friction for the three coarsest grid densities. Across the two finest grid densities the WA-QCR model sees a sudden increase in skin friction while the SA-QCR model experiences a modest increase. At the finest grid the use of QCR results in better agreement for both models, however agreement between the WA-QCR and experimental results is still somewhat poor. On the other hand, the SA-QCR model shows good agreement with experimental friction.

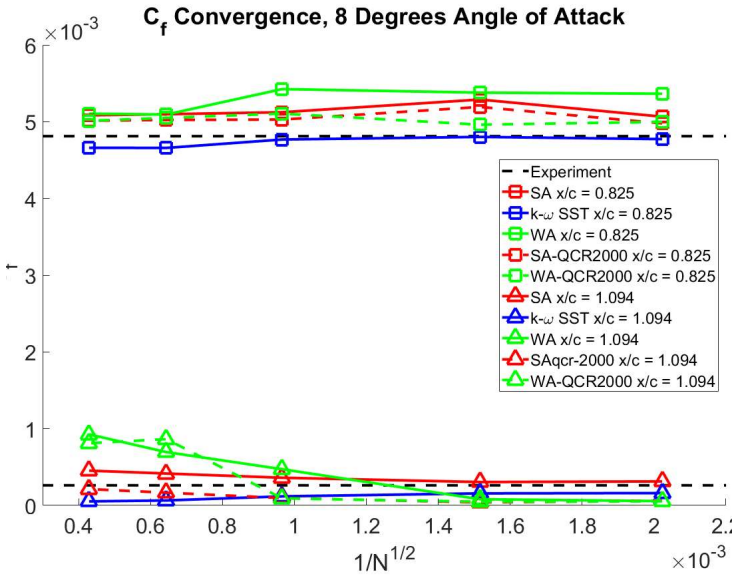


**Figure 6 Convergence history of skin friction coefficient on the main element (x/c = 0.825) and flap (x/c = 1.094) on five grid levels using SA, SST k-ω, WA, SA-QCR2000, and WA-QCR2000 models and their comparison with experiment (dotted line).**

The computed coefficient of pressure is compared to experimental results from Chin et al. [13] in Figure 7. Both the SA and SST *k-ω* turbulence models show good agreement with the experimental results with the former slightly over-predicting the magnitude of the suction peak and the latter slightly under-predicting it. Solutions computed using the WA model show a slight but significant under-prediction of the suction peak. The use of QCR results in only a very minor effect on computed results along the flap and along the whole wing (not shown). At the

suction peak, the use of QCR with the SA model leads to a slight decrease in the magnitude of the pressure coefficient and results in very good agreement with experimental results. Use of QCR with the WA model does not produce a significant change in the pressure.

The comparison of the skin friction coefficient on the 30P30N between the experimental results from Klausmeyer and Lin [16] and the computations using each turbulence models on the very fine grid is shown in Figure 9. Along the suction side of the wing, the WA model predicts the highest level of skin friction, while the SST *k-ω* model predicts the lowest level. Along the slat, both the WA and SA models show a similar level of agreement with the experimental results, albeit with the former over-predicting and the latter under-predicting. Along the main element all three turbulence models show good agreement with the experimental results. Immediately downstream of the flap suction peak, all three turbulence models under-predict the skin friction compared to experimental results with the WA model predicting the closest levels of skin friction. Towards the trailing edge of the flap, the SA and WA models show good agreement with experimental results on the suction side while the SST *k-ω* model slightly underpredicts values.

Along the pressure side of the flap all three turbulence models under-predict the skin friction. The use of QCR has no noticeable effect on the skin friction along the slat and in the immediate vicinity of the suction peak of the main element. Further downstream the WA-QCR predicts a slight decrease in skin friction, which brings the model into very good agreement with experimental results. A similar effect is not seen for the SA model. Immediately downstream of the flap suction peak the use of QCR with the WA model results in a decrease in the measured friction while friction is increased further downstream, near the trailing edge. This indicates slightly better attachment is predicted by the WA-QCR model compared to the base linear model. The use of QCR with the SA model results in a decrease in skin friction across most of the suction side of the flap. Along the pressure side of the flap, QCR results in a decrease in skin friction for the WA model while use with the SA model results in very little difference.

Profiles of velocity magnitude and Reynolds shear stress are shown along a series of lines on the upper side of the flap and are compared to experimental values from Chin et al [13] and Mcginley et al. [17]. The axes for the Reynolds stress tensor are chosen to match the local streamline such that $u$ is tangent to the streamline and $v$ is normal to it [5]. This is achieved using the coordinate transformation in Equation 5.1.1 where $\theta$ represents the angle of the flow.

$$-u'v'|_\theta = -u'v'\cos(2\theta) + 0.5(u'u' - v'v')\sin(\theta) \tag{10}$$

The location of these lines is shown in Figure 8 and the comparisons between the computed results from each turbulence model and experimental data are shown in Figure 10 through Figure 13. Along the line x/c = 0.717 a sharp change is observed in the experimental Reynolds stress profile near to the wall. This is most accurately predicted by the WA and SST *k-ω* models while the SA model predicts the change at approximately half the distance to the wall. Slightly farther from the wall a peak in Reynolds stress can be observed. From the plot of velocity at the same location it can be seen that this occurs at the center of the main element wake. All three linear turbulence models greatly over-predict the magnitude of this peak, with the SA model showing the poorest agreement. However, both the SA model and WA model using QCR show very good

agreement with the experimental Reynolds stress in this section. Slightly further from the wall a sharp minimum is measured in the experimental results. Neither the linear nor the nonlinear turbulence models accurately predict this feature, however a slight improvement is seen in both QCR models over their base linear models. Beyond this section the experimental Reynolds stress remains effectively constant while a small bump is predicted by all three models in line with the slat wake. This bump is smallest for the WA and SST *k-ω* models and noticeably greater for the SA model. The use of QCR has a limited effect on the size and shape of this bump.

The velocity profile at the same location shows the SA and SST *k-ω* to be in best agreement with experimental results in the main element wake while all three models over-predict the magnitude of the slat wake. QCR results in small improvement in the wakes of both elements predicted by the WA model, but it is inconsequential otherwise. At x/c = 0.87 the sharp change in Reynolds stress is once again predicted by the WA and SST *k-ω* turbulence models, however it does not appear in the experimental results. Further from the wall the SA-QCR model shows good agreement with the magnitude and location of the stress peak while the base SA model and the other turbulence models under-predict it. All three turbulence models predict a large decrease in the Reynolds stress at the main element outer half wake, but this is not seen in experimental measurements which instead return roughly to zero. Once again, a small bump is erroneously predicted by all three turbulence models in the slat wake section with the WA model showing the closest agreement to the experimental profile. All three turbulence models show good agreement with the velocity profile at the same location within the boundary layer, however only the SA model is in good agreement with experimental results in the main element wake. Likewise, the SA model shows the closest agreement to experimental results in the slat wake, however all three once again over-predict its influence.

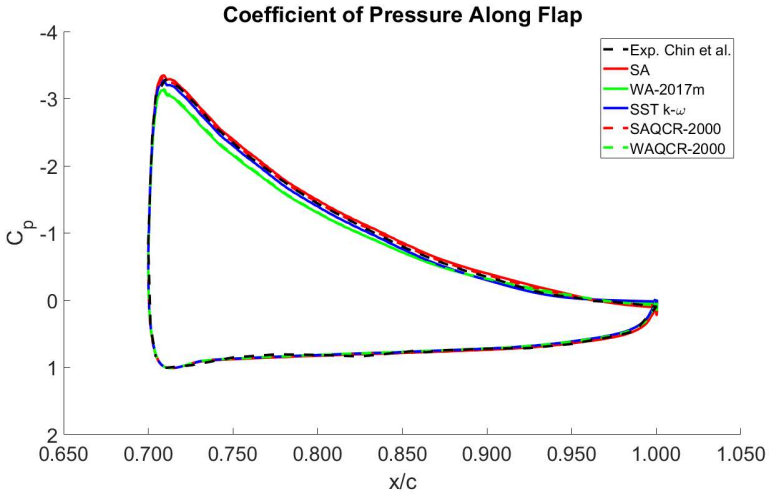


**Figure 7 Coefficient of pressure along flap for SA, SST k-ω, WA, SA-QCR2000, and WA-QCR2000 turbulence models, 8 degrees angle of attack**

Only velocity profile data is available at x/c = 0.925. As has been seen previously all three turbulence models show good with experimental results along the boundary layer but only the SA model is in good agreement in the main element wake. The Reynolds shear stress profile at x/c = 0.975 shows good agreement between the WA model within the boundary layer section of

the flow. This agreement is further improved by the use of QCR. On the contrary the SA model under-predicts the magnitude of the Reynolds stress in the boundary layer and QCR resulting in further decreased accuracy. Further from the wall the SA model shows the best agreement with experimental stress, however the use of QCR causes the stress to be greatly over-predicted. Along the main element outer half wake the decrease in the stress is once again over-predicted, however not as poorly as in the previous section. Along the slat wake section, the WA model is in good agreement while the SA model continues to erroneously predict a bump. Outside of the boundary layer and main element wake QCR has a negligible effect on the Reynolds stress for either model. The velocity profile at the same location shows good agreement between the WA and SA models and experimental results within the boundary layer, however the near-zero velocity predicted away from the wall by the SST $k$-$\omega$ model indicates a region of local recirculation. Further from the wall the SA model is once again in the best agreement with experimental results with the WA model over-predicting the magnitude of the slat and main element wake.

In all but one case the use of QCR results in a Reynolds shear stress profile that is either similar or improved to its corresponding linear profile. Despite this, QCR does not result in a noticeable improvement in the computed velocity profiles. Furthermore, when one model does show a noticeable improvement over the others in predicting the Reynolds stresses, this did not necessarily result in a better prediction of the velocity profile. This is most apparent in the slat wake zone where the WA model consistently predicts the most accurate stress profile while the SA model predicts the least accurate. However, in the velocity profile the results are reversed, with the former showing poor agreement with experimental results and the SA model showing the closest agreement (albeit still with significant differences). Combined with the limited differences observed in most other aspects of the flow, the use of QCR is judged to have limited effect in computing 2D high-lift flows. However, because there is little detriment observed in the utilization of QCR, and because the implementation of QCR requires only a small increase in computational resources, its use can still be considered beneficial. Furthermore, the added complexity of 3D flows, namely the corner flow at the wing-root, means QCR still has high potential to be an effective tool in the prediction of high-lift flows. Indeed, the fact that QCR had a limited effect on flow past a comparatively simple geometry, where linear turbulence models were already in reasonable agreement with the experimental flow, means that implementing QCR may be able to improve poorly predicted regions while leaving well predicted regions mostly unaffected. As such, the analysis of QCR on 3D geometries is an important next step towards evaluating its potential in predicting high-lift flows.

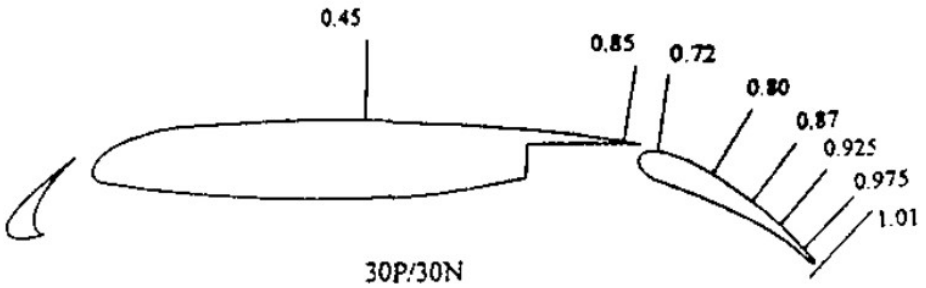


**Figure 8 Flow field survey locations x/c**

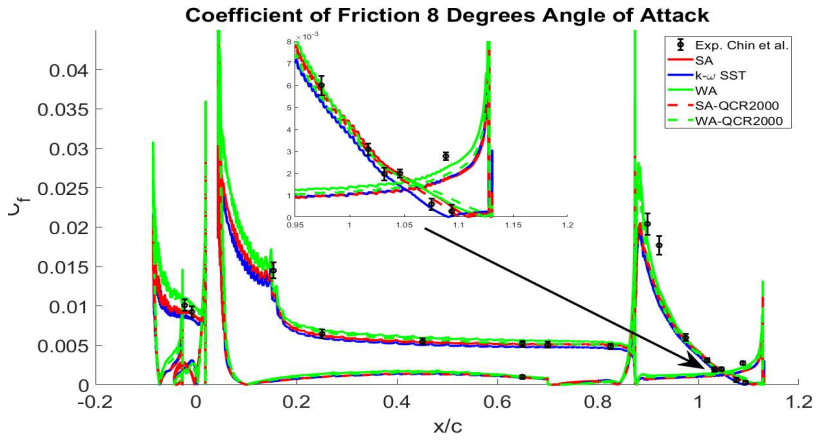


**Figure 9 Comparison of computed skin friction coefficient on all three elements using SA, SST k-ω and WA turbulence models and experimental data**

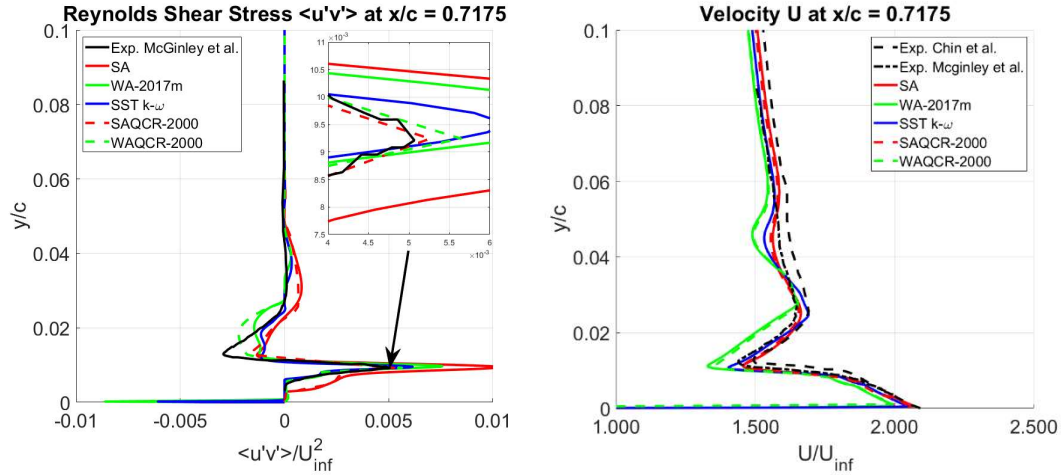


**Figure 10 Plots of (u'v')⁻/U_∞^2(left) and U/U_∞ (right) along upper side of flap, at x/c = 0.717, for SA, SST k-ω, WA, SA-QCR2000, and WA-QCR2000 turbulence models, 8 degrees angle of attack**

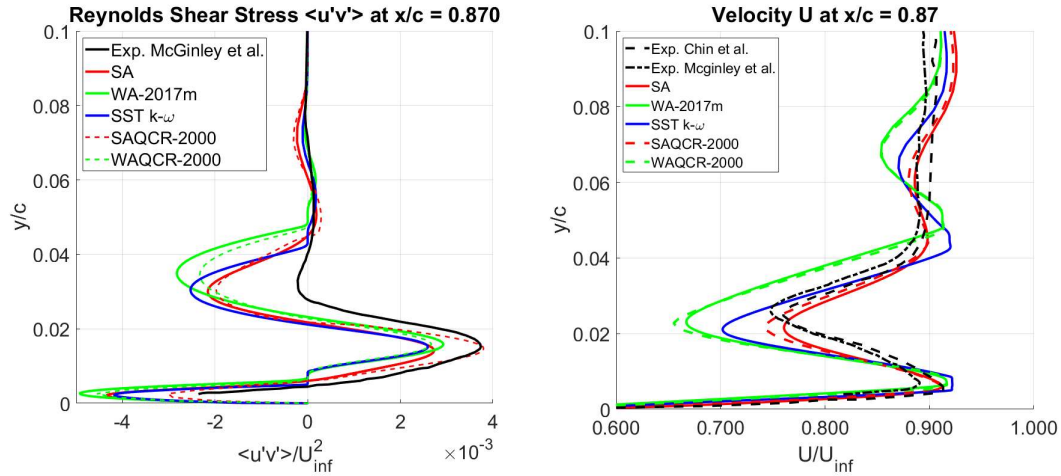


**Figure 11 Plots of (u'v')⁻/U_∞^2(left) and U/U_∞ (right) along upper side of flap, at x/c = 0.87, for SA, SST k-ω, WA, SA-QCR2000, and WA-QCR2000 turbulence models, 8 degrees angle of attack**

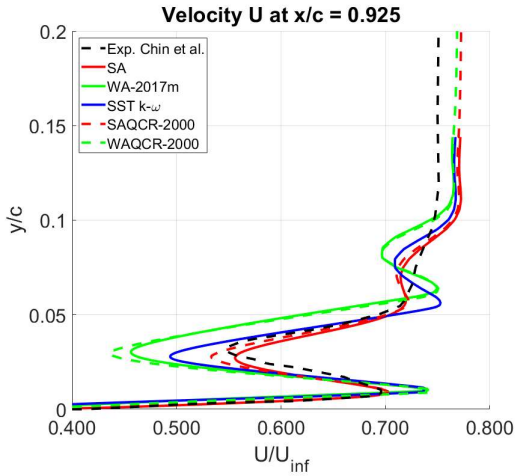


**Figure 12 U/U∞ along upper side of flap, at x/c = 0.925, for SA, SST k-ω, WA, SA-QCR2000, and WA-QCR2000 turbulence models, 8 degrees angle of attack**

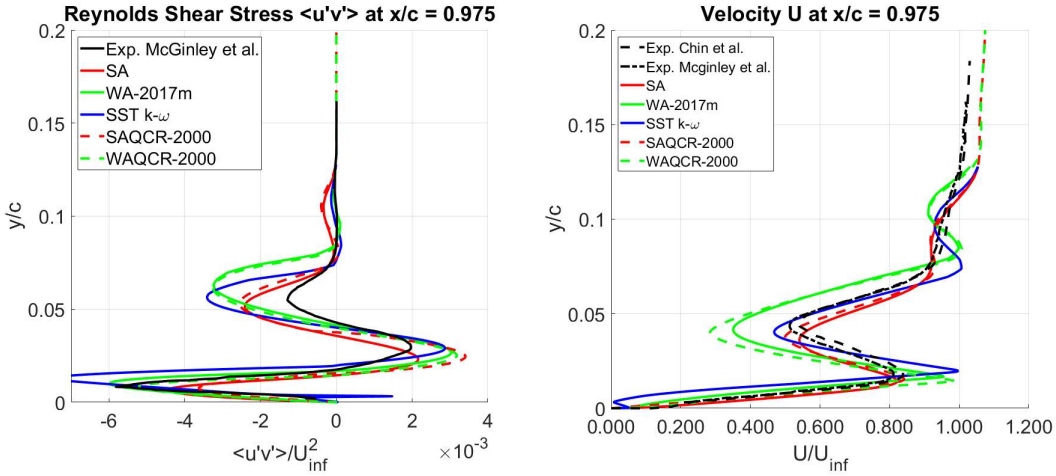


**Figure 13 Plots of (u'v')⁻/U_∞^2(left) and U/U_∞ (right) along upper side of flap, at x/c = 975, for SA, SSTk-ω, WA, SA-QCR2000, and WA-QCR2000 turbulence models, 8 degrees angle of attack**

## Conclusion

Computations were performed on 30P30N three-element airfoil using the three turbulence models – SA, SST *k-ω* and the recently developed Wray-Agarwal one equation turbulence to evaluate their relative accuracy. The analysis included a grid independence study, and comparison of various flow field variables and aerodynamic coefficients for a wide range of angles. The grid independence study found that for the coefficient of lift the SA model achieved grid independence of the solution on the coarsest mesh while the SST *k-ω* and WA models required finer meshes for grid independence of the solution. However, at higher mesh densities the WA and SST *k-ω* turbulence models showed better agreement with experimental lift values than the SA model. The mesh independence study for skin friction showed that along the trailing edge of the main element, each turbulence model reached grid independence at a similar level of mesh density and each model showed a similar level of agreement with experimental results. The mesh independence study also showed that all three turbulence models had decreased accuracy in the predicted lift coefficient compared to experimental results as mesh density increased.

Evaluation of the coefficient of pressure along the flap at 8 degree angle of attack showed that all three turbulence models showed good agreement with experimental measurements. The SA model overall showed the best accuracy; however, the WA model showed similar accuracy towards the trailing edge of the flap. A comparison of the skin friction showed that all three turbulence models showed good agreement with experimental results away from each element's suction peak. Close to the suction peak the turbulence models under-predicted the skin friction coefficient. In these regions the WA model results were closest to the experimental values.

The Quadratic Constitutive Relation was used for the SA and WA models to gauge its effect on two-dimensional high lift flows. Slight variations were observed in the lift and drag as the grid density increased. The use of QCR resulted in a small decrease in the total lift. Additionally, QCR gave an improved prediction of skin friction along two sections of the wing. A full comparison of the coefficients of pressure and skin friction found a negligible change in the former and a slight improvement along certain sections of the wing in the latter. Finally, profiles of Reynolds stresses and velocity above the flap were evaluated using QCR and compared to results generated using linear turbulence models. The use of QCR resulted in modest improvements in the predicted Reynolds stresses along certain sections of the profile; however, little change was observed in the corresponding velocity profiles, indicating an accurate prediction of Reynolds stresses is not sufficient in the accurate prediction of wake boundary layer mixing.

**Acknowledgement**
Funding for this project was provided by NASA Missouri Space Grant Consortium Grant Award number 80NSSC20M0100.

**Biography**
Karsten Hendrickson is a PhD candidate at Washington University in St. Louis. Karsten is originally from Seattle, Washington. He received a Bachelor's of Science in Applied Physics from Pacific Lutheran University and a Master of Science in Aerospace Engineering from WUSTL. His research in computational fluid dynamics includes modeling of high lift systems and active flow control.

**References**

[1] Rumsey, C. L., and Ying, S. X. "Prediction of High Lift: Review of Present CFD Capability." *Progress in Aerospace Sciences*, Vol. 38, No. 2, 2002, pp. 145–180. https://doi.org/10.1016/S0376-0421(02)00003-9.

[2] Rumsey, C. L., Slotnick, J. P., and Sclafani, A. J. Overview and Summary of the Third AIAA High Lift Prediction Workshop. No. 56, 2019, pp. 621–644.

[3] Ashton, N., West, A., and Mendonça, F. Flow Dynamics Past a 30P30N Three-Element Airfoil Using Improved Delayed Detached-Eddy Simulation. No. 54, 2016, pp. 3657–3666.

[4] Takeda, H., Yamamoto, T., and Hayashi, K. *FaSTAR 30P30N Computation of 30P30N in Various Turbulence Models by FaSTAR Code*. 2019.

[5] Ying, S. X., Spaid, F. W., McGinley, C. B., and Rumsey, C. L. “Investigation of Confluent Boundary Layers in High-Lift Flows.” *Journal of Aircraft*, Vol. 36, No. 3, 1999, pp. 550–562. https://doi.org/10.2514/2.2490.

[6] Bario, F., Charnay, G., and Papailiou, K. D. “An Experiment Concerning the Confluence of a Wake and a Boundary Layer.” *Journal of Fluids Engineering*, Vol. 104, No. 1, 1982, pp. 18–23. https://doi.org/10.1115/1.3240845.

[7] Rumsey, C. L., Lee-Rausch, E. M., and Watson, R. D. “Three-Dimensional Effects in Multi-Element High Lift Computations.” *Computers & Fluids*, Vol. 32, No. 5, 2003, pp. 631–657. https://doi.org/10.1016/S0045-7930(02)00032-4.

[8] Han, X., Wray, T., and Agarwal, R. K. Application of a New DES Model Based on Wray-Agarwal Turbulence Model for Simulation of Wall-Bounded Flows with Separation. 2017.

[9] Spalart, P. R. “Strategies for Turbulence Modelling and Simulations.” *International Journal of Heat and Fluid Flow*, Vol. 21, No. 3, 2000, pp. 252–263. https://doi.org/10.1016/S0142-727X(00)00007-2.

[10] Wray, T. J., and Agarwal, R. K. “Low-Reynolds-Number One-Equation Turbulence Model Based on k-ω Closure.” *AIAA Journal*, Vol. 53, No. 8, 2015, pp. 2216–2227. https://doi.org/10.2514/1.J053632.

[11] Antoniadis, A. F., Tsoutsanis, P., and Drikakis, D. Numerical Accuracy in RANS Computations of High-Lift Multi-Element Airfoil and Aircraft Configurations. 2015.

[12] Rumsey, C. 3rd AIAA CFD High Lift Prediction Workshop Gridding Guidelines. https://hiliftpw.larc.nasa.gov/Workshop3/GriddingGuidelines-HiLiftPW3-v10.pdf. Accessed Nov. 1, 2020.

[13] Chin, V. D., Peters, D. W., Spaid, F. W., and McGhee, R. J. Flowfield Measurements about a Multi-Element Airfoil at High Reynolds Numbers. 1993.

[14] Rumsey, C. L., Slotnick, J. P., Long, M., Stuever, R. A., and Wayman, T. R. “Summary of the First AIAA CFD High-Lift Prediction Workshop.” *Journal of Aircraft*, Vol. 48, No. 6, 2011, pp. 2068–2079. https://doi.org/10.2514/1.C031447.

[15] Rumsey, C. L., and Slotnick, J. P. “Overview and Summary of the Second AIAA High-Lift Prediction Workshop.” *Journal of Aircraft*, Vol. 52, No. 4, 2015, pp. 1006–1025. https://doi.org/10.2514/1.C032864.

[16] Klausmeyer, S., and Lin, J. An Experimental Investigation of Skin Friction on a Multi-Element Airfoil. 1994.

[17] McGinley, C. B., Anders, J. B., and Spaid, F. W. Measurements of Reynolds Stress Profiles on a High-Lift Airfoil. 1998.